Calibration of Surface Science Lamp Flux

By M. Tomasko, L. McFarlane, and B. Rizk

Table of Tables

Table of Figures

This document describes the determination of the flux output from the Surface Science Lamp (SSL)on the DISR03 flight unit. We begin by describing the general approach. This is followed by tables and plots that give the spectral distribution of the flux of the SSL as well as the spatial distribution of the SSL.

The general approach to determining the output of the SSL is as follows. We require knowledge of the field of view of the Downward Looking Infrared Spectrometer (DLIS), as well as the wavelength and responsivity of each pixel of the DLIS. The SSL was used to illuminate a target while the DLIS recorded a spectrum of the light reflected from the target and the DISR imagers obtained images of the pattern of light on the target. We need to know the parallax between the DISR imagers and the geometry and responsivity of the imagers in order to determine the relative spatial pattern of the SSL. A calibrated laboratory spectrometer was used with a standard lamp to measure the reflectivity of the target. Finally, knowing the integral of the relative spatial pattern of the lamp over the field of view of the DLIS permits the absolute intensity measured by the DLIS at each pixel in its spectrum to be converted to the brightness of the target at the location of the peak of the brightness pattern as a function of wavelength. Together with the reflectivity of the target as a function of wavelength, this gives the absolute spectral output of the SSL as a function of wavelength at the peak of the pattern of the SSL. The parallax between the pattern of the SSL and the field of view of the DLIS can be corrected to the situation at Titan when the range to the target is essentially infinite, and the count rate at each DLIS pixel can be computed as a function of altitude for Titan surfaces having any reflection spectrum. Finally, the scattered light from the SSL into the DLIS from scattering paths within the DISR instrument was measured during the same series of tests used for the determination of the brightness of the SSL. The amount of scattered light expected can be added to the measurements of light reflected from the surface of Titan, and the resulting total count rate in each pixel as functions of altitude and surface reflectivity can be derived to estimate the signal to noise ratio of the Titan measurements.

We begin with the determination of the field of view of the DLIS. This was measured using the DISR sensor head mounted on the altitude-azimuth mount and illuminated with the beam of light from the collimator. Three scans were made: two in azimuth with the zenith angle of the source at 157 and 161 degrees, respectively, and one in zenith with the azimuth angle set at zero degrees. The size of the aperature over the source was 1/8 inch at the focus of the 72 inch focal length spherical mirror of the collimator. This corresponds to a collimation of the light beam from the collimator to a full angle of 0.0995 degrees, less than 0.1 degree. The three cuts across the field of view of the DLIS are shown in Figs. 1. and 2.

The three cuts across the field of view (FOV) of the DLIS can be used to determine the location of the center of the slit, its orientation, and its length and width. To do this, it is useful to transform from a rectangular right-handed coordinate system with the x axis horizontal pointing outward at zero azimuth and the z axis vertical to a primed system tipped so that the x’ axis points outward along the center of the FOV of

the DLIS an with the z' axis tipped in the plane at zero azimuth. The two coordinate systems are shown in Fig. 3. This transformation is useful because the normal location of

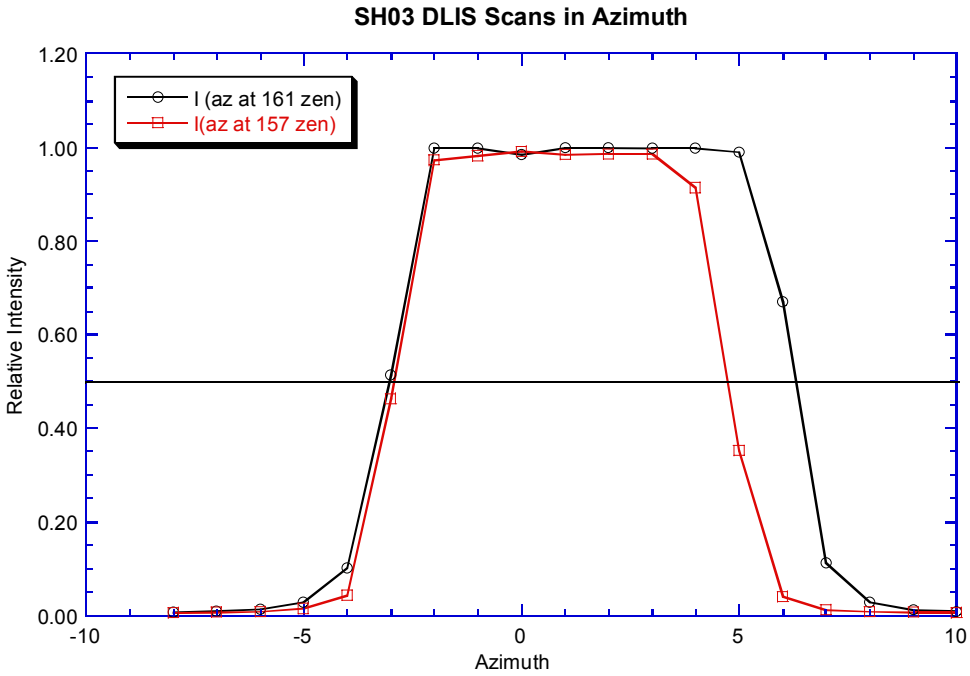

Fig. 1 Relative intensity in DLIS spectrum in two cuts across the slit in azimuth at fixed zenith angles are shown. This information along with the zenith angle cut from Fig. 2 below are sufficient to determine the size and location of the DLIS slit.

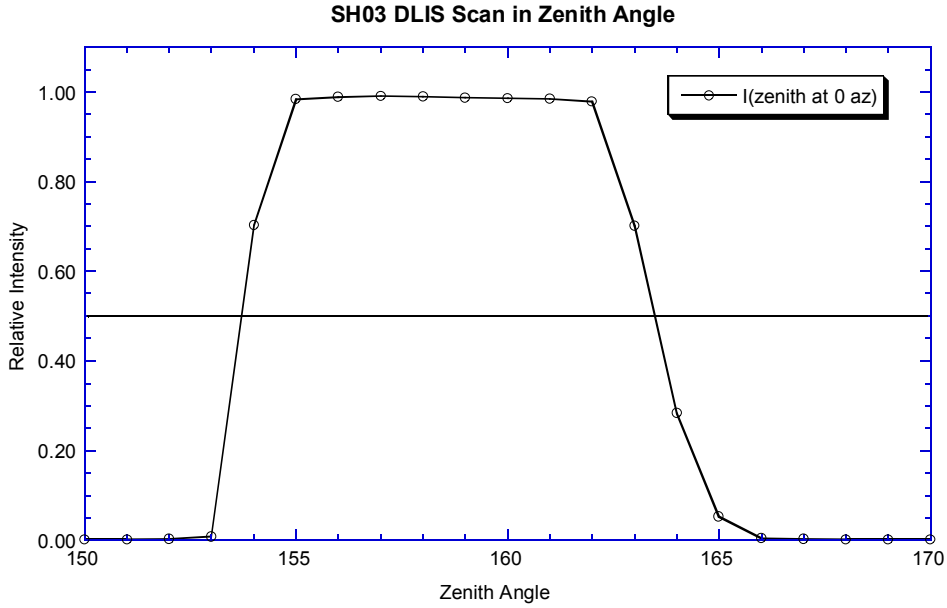

Fig. 2 Relative intensity in the DLIS spectrum in a cut in zenith at constant azimuth angle is shown.

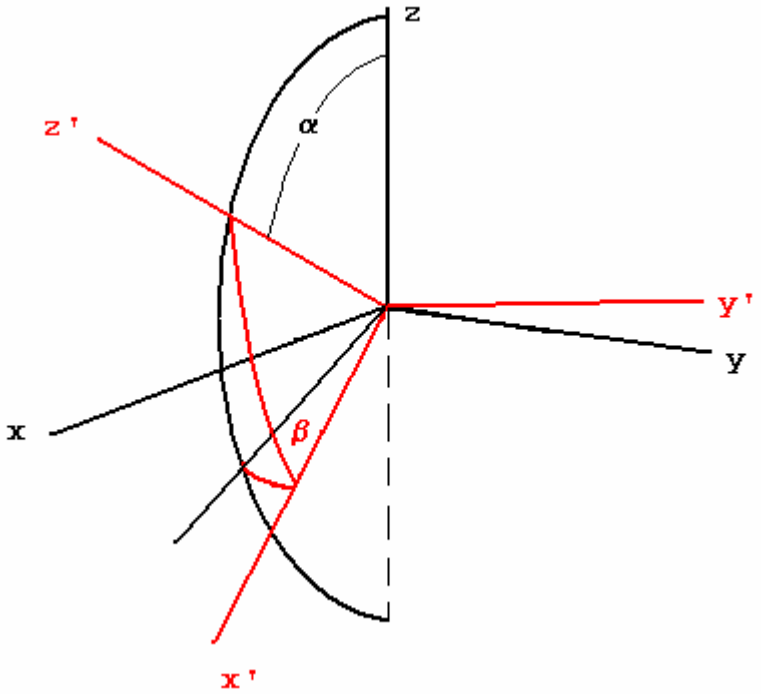

Fig. 3 The relationship between an x-y-z coordinate system in which z is vertical and x points in the direction of zero azimuth and an x'-y'-z' coordinate system in which x' points in the direction of the center of the DLIS field of view, z' is in the plane of zero azimuth, and y' is perpendicular to x' and z'. Angle α is 68.6 degrees and β is 0.42 degrees.

slit is at a zenith angle of some 160 degrees, only 20 degrees from the pole of the spherical coordinate system. After the transformation, the center of the slit is at the equator of a spherical coordinate system, and the distortion of the slit is less severe.

It turns out that the slit is slightly rotated about an axis along the center of the FOV, and so a second coordinate transformation of coordinates to accommodate this rotation is desirable. Figure 4 shows this second transformation. The relations between coordinates in the primed and unprimed systems are as follows. The unit vector in the primed system is given in terms of the angles α_0 and β_0 as follows:

$$\begin{aligned}
\hat{i}' &= \sin(\beta_0)\hat{j} + \cos(\beta_0)\cos(\alpha_0)\hat{i} - \cos(\beta_0)\sin(\alpha_0)\hat{k}\,, \\
\hat{j}' &= -\cos(\alpha_0)\sin(\beta_0)\hat{i} + \cos(\beta_0)\hat{j} + \sin(\alpha_0)\sin(\beta_0)\hat{k} \\
\hat{k}' &= \sin(\alpha_0)\hat{i} + \cos(\alpha_0)\hat{k}\,.
\end{aligned} \qquad (1.)$$

The unit vectors in the primed system are given relative to the double primed system by

$$\begin{aligned}
\hat{i}' &= \hat{i}'' \\
\hat{j}' &= \cos(\vartheta)\hat{j}'' - \sin(\vartheta)\hat{k}''
\end{aligned} \qquad (2.)$$

$$\hat{k}' = -\sin(\vartheta))\hat{j}'' + \cos(\vartheta)\hat{k}'' .$$

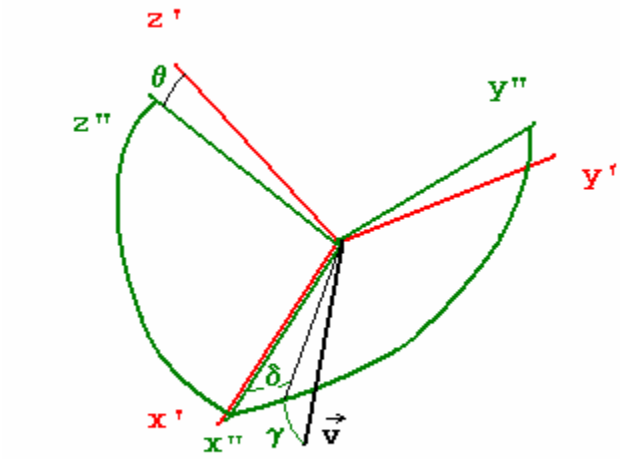

Fig. 4 The relationship between the x'-y'-z' and the rotated x"-y"-z" coordinate systems is shown. The double primed system has been rotated θ degrees counterclockwise about the x' axis. The vector v in the double primed system is located δ degrees from the x" axis in the x"-y" plane and γ degrees below the x"-y" plane.

Now the location of the boundaries of the slit in the double primed system are simply given by vectors v located plus and minus d degrees from the x" axis and g degrees above and below the x"-y" plane, as shown in Fig. 4. One corner is located at the vector v shown in Fig. 4, and its coordinates in the double primed system are

$$\vec{v} = \cos(\gamma)\cos(\delta)\hat{i}'' + \cos(\gamma)\sin(\delta)\hat{j}'' - \sin(\gamma)\hat{k}'' . \qquad (3.)$$

Equation (2) can be used with equation (3) to give the coordinates of the edges of the slit in the primed coordinate system, and equation (1) can be used with the result to give the location of the slit in the original unprimed coordinate system. When this is done, the unprimed coordinates can be used to find the zenith angle (ZA) and the azimuth angle (AZ) of the boundaries of the slit. We have

$$ZA = \cos^{-1}(z),$$
$$AZ = \tan^{-1}(y/x) \qquad (4.)$$

where the x, y, and z are the components of the vector to the slit boundary in the unprimed system.

Collecting these the location of the slit in these three coordinate systems permits computations as shown in Fig. 5. In the third panel of this figure, we see the outline of the slit in azimuth and zenith angle compared with the half-power points from Figs 1 and

2 shown in red. The outline of the slit is in good agreement with the constraints of Figs 1 and 2 for the location, size, and orientation of the DLIS slit given in Table 1.

Table 1
Location, Size, and Orientation of DLIS Slit

Parameter	Value(degrees)
α_0	68.6
β_0	0.42
θ	2.42
Slit Length	9.77
Slit Width	3.006

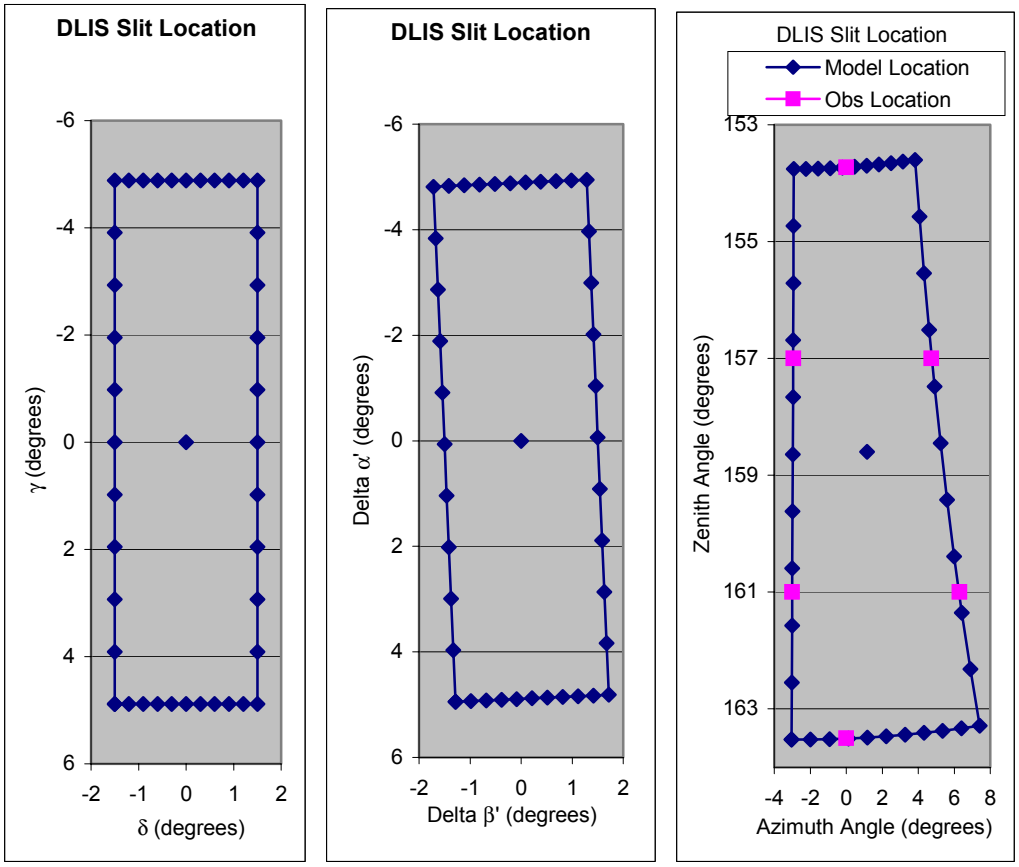

Fig. 5 The left panel shows the location of the slit in the double primed system, the center panel shows the location in the single primed system, and the right panel shows the location in an azimuth, zenith angle system in the unprimed system. In the right panel, the red points show the half-power points in the slit scans of Figs. 1 and 2. These points are in good agreement with the outline of the slit determined here for the size and orientation of the slit as given in Table 1.

The spatial distribution of the SSL was determined by DISR images of a target while the target was illuminated by the SSL. The target consisted of a large flat sheet of

anodized aluminum that contained small squares painted with black Krylon paint. These small painted areas contained small slits that were used in the imager line spread function test. Despite the fact that the target contained two different types of material, images of the target made with the DISR imagers can be used to determine the spatial distribution function of the SSL. Knowing the spatial distribution function for the output of the lamp, the DLIS spectra of the target permit determination of the spectral output of the lamp so long as the spectrum of the lamp is assumed to be independent of direction.

In addition to the location of the field of view of the SSL, we next need to know the reflectivity of the target that was illuminated by the SSL and observed by the DLIS. This target was a large sheet of black anodized aluminum that contained small squares painted with flat black Krylon spray paint. The target was constructed for use in our measurement of the line spread function of the imagers, and in each of the several small black Krylon squares we built slits to provide line spread sources. For the SSL measurement, the size of the Krylon portions of the target contribute only a percent or two of the field of view illuminated by the SSL and observed by the DLIS. We correct for the dual nature of the target by measuring the reflectivity of both the anodized portion of the target and the Krylon portion of the target separately. For this measurement the targets were illuminated by a lamp and viewed by a monochrometer followed by a standard detector. For reference, we viewed the inside of the front cover of our Labsphere integrating sphere. This cover is eight inches in diameter and is painted with Spectraflect, as is the inside of our 20 inch diameter integrating sphere. The reflectivity of the spectraflect surface of the cover is listed as having the reflectivities given in Table 2. These numbers form the primary standard to which the output of the lamp is measured.

Table 2
Reflectivity of Spectraflect surface as a Function of Wavelength

Wavelength (nm)	Reflectivity	Wavelength (nm	Reflectivity
400	0.983	1150	0.982
450	0.984	1200	0.970
500	0.983	1250	0.975
550	0.984	1300	0.972
600	0.983	1350	0.963
650	0.983	1400	0.944
700	0.984	1450	0.909
750	0.984	1500	0.919
800	0.982	1550	0.930
850	0.984	1600	0.931
900	0.981	1650	0.940
950	0.981	1700	0.938
1000	0.983	1750	0.928
1050	0.982	1800	0.917
1100	0.981	1850	0.901

In order to measure the reflectivity of the anodized aluminum and Krylon painted portions of the target, we illuminated the target by the high-intensity lamp from a direction perpendicular to the target. We used the monochrometer followed by the standard silicon and germanium detectors to measure the light reflected from the target.

We then substituted the spectraflect cover for the target and repeated the measurements. The ratio of the signals gives the reflectivity of the target compared to that of spectraflect.

These measurement were repeated with the monochrometer source located at various angles from the direction of lamp illumination. We performed the measurements at angle of 4, 18, 36, and 52 degrees from the normal to the surface of the targets. While the signals from the spectraflect target and the flat black Krylon painted targets were relatively independent of observation angle, the measurements of the anodized aluminum target contained a significant component due to specular reflection, and varied considerable with observation angle. The raw ratios as a function of wavelength are shown in Fig. 6.

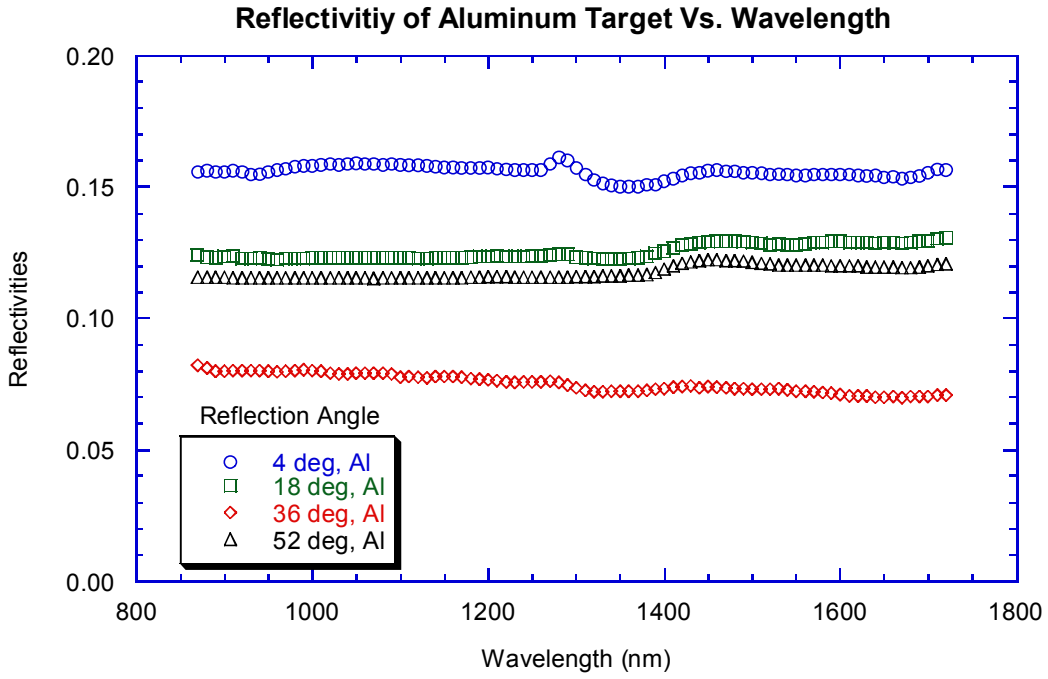

Fig. 6 Measured reflectivity of the anodized aluminum target illuminated normal to the target and observed at various observation angles from the normal, as labeled. The observed ratio of brightness from the target to the brightness of the spectraflect cover varies appreciably with observation angle.

The variation of measured reflectivity with observation angle is shown in Fig. 2 at several wavelengths for the aluminum target. Figure 3 shows an enlargment of the region of Fig. 7 at small observation angles. From 4 degrees to 0 degrees observation angle the reflectivity changes by only about 1%, relatively independent of wavelength. The DISR observations of the targets will be within about 2 degrees of normal when the targets are normally illuminated. We adopt the measurements made at 4 degrees from normal for use in our reductions. We take the reflectivity of the targets as the product of the measured reflectivity relative to the spectraflect cover times the published reflectivity curve of Table 2 for spectraflect.

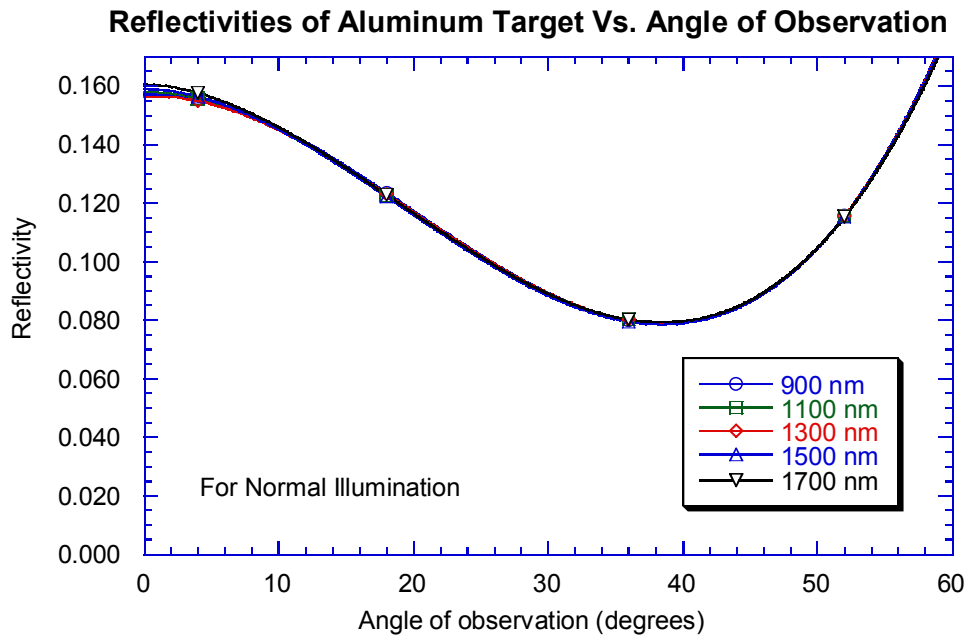

Fig. 7 The reflectivity of the anodized aluminum target measured relative to the spectraflect cover as a function of the angle of observation for five wavelengths. The targets were illuminated normal to the surface of the targets.

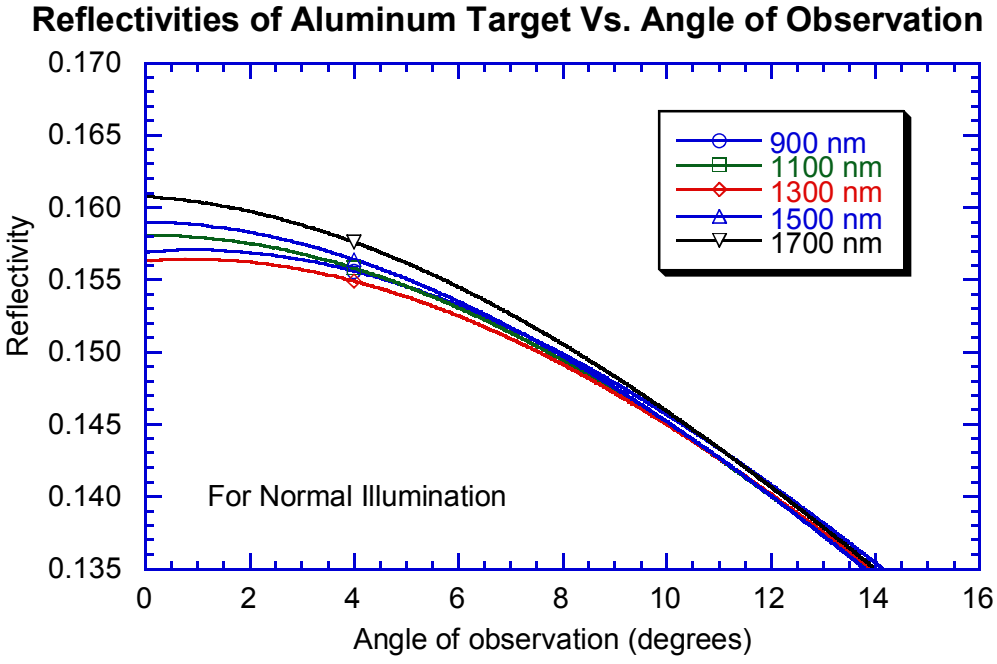

Fig. 8 Enlargement of the region at small angles of scattering of Fig.7. Note that the measured reflectivity of the anodized aluminum target changes by only about 1% in the region between 0 and 4 degrees observation angle. The

DLIS observations are at observation angles of a few degrees. We adopt the measurements at 4 degrees for our reductions.

The relative spatial output of the lamp can be determined as follows. We assume that the spectraflect target is lambertian, that is the intensity from the spectraflect target is

$$\pi I_{specrraflect}(\lambda,\phi,\varphi) = \mathbf{F}_{Lamp}(\lambda,\phi,\varphi) R_{spectraflect}(\lambda) \qquad (5.)$$

where $R_{spectraflect}(\lambda)$ is the reflectivity of the spectraflect target. The ratio of the intensity observed from the anodized aluminum target to that of the spectraflect target was measured as R_{Al} at an observation angle similar to that used when DISR observed the combined target. The intensity that would be observed from an entirely anodized aluminum target illuminated by the SSL is thus given by

$$I_{target}(\lambda,\vartheta,\varphi) = R_{spectraflect} R_{Al} \mathbf{F}_{SSL}(\lambda) F'(\vartheta,\varphi)/\pi \, . \qquad (6.)$$

Here we have also assumed that the lamp flux dependence on wavelength and spatial direction are separable, or

$$\mathbf{F}_{Lamp}(\lambda,\vartheta,\varphi) = \mathbf{F}_{p}(\lambda) F'(\vartheta,\varphi) \qquad (7.)$$

where $F'(\vartheta,\varphi)$ is the relative spatial distribution of the lamp flux and $\mathbf{F}_P(\lambda,)$ is the wavelength distribution of the lamp flux at the peak of the spatial distribution. Thus the intensity of light reflected from a portion of the surface covered by material with reflectivity $R(\lambda)$ is given by

$$I(\lambda,\vartheta,\varphi) = \mathbf{F}_{P}(\lambda) F'(\vartheta,\varphi) R(\lambda)/\pi \, . \qquad (8.)$$

where R(l) is the product of the spectraflect reflectivity and the ratio of intensities measured for the target material to that measured from the spectraflect target. The net count rate in DN/sec measured by the imager is given by

Microsoft Equation 3.0

$$DN/\sec = Resp_{peak}(\vartheta,\varphi) \int I(\lambda,\vartheta,\varphi) Rel(\lambda) d\lambda \qquad (9.)$$

where $Rel(\lambda)$ is the relative spectral response of the imager normalized to unity at the wavelength of the peak response and $Resp_{peak}(\vartheta,\varphi)$ is the responsivity at the peak of the relative spectral response curve in the direction specified by θ and ϕ. Inserting (8) into (9) gives

$$DN/\sec = Resp_{peak}(\vartheta,\varphi) F'(\vartheta,\varphi) \int \mathbf{F}_{P}(\lambda) R(\lambda) Rel(\lambda) d\lambda/\pi \, . \qquad (10.)$$

Equation (10) can be solved for the relative spatial distribution of the lamp flux as

$$F'(\vartheta,\varphi) = \pi \frac{DN/\sec}{Resp_{peak}(\vartheta,\varphi)\int \mathbf{F}_P(\lambda,)R(\lambda)Rel(\lambda)d\lambda}. \qquad (11.)$$

As mentioned above, the target used in the measurement of the SSL flux contained two different reflectivities: most of the target was black anodized aluminum, and the small squares were painted with flat black Krylon paint. The relative response derived for the Krylon and the anodized surface will be different by a factor given by the integral in the denominator of equation (11). Actually, the reflectivities of both the Krylon and the anodized surface are relatively constant over the spectral range of the DISR imagers, so even a crude estimate of the relative spectral output of the lamp will permit determination of the factor by which measurements of the relative spatial distribution of the lamp in the small Krylon squares must be multiplied to put them on the same scale as for the anodized surface. Table 3 below contains the reflectivities of the Krylon and anodized surface as well as the relative spectral response of the Medium Resolution Imager (MRI) on DISR03. Also included in the relative shape of the flux with wavelength from a black body at a temperature of 3186 K.

Table 3
Functions needed to Estimate the Relative Brightness in the MRI imager of Anodized Aluminum and Painted Krylon Surfaces

Wavelength (nm)	Reflectivity of Krylon	Reflectivity of anodized aluminum	Relative spectral Response	Relative Lamp Flux
600	0.0331	0.1613	0.0005	0.604
610	0.0332	0.1612	0.0004	0.633
620	0.0332	0.1611	0.0004	0.660
630	0.0333	0.1612	0.0006	0.686
640	0.0332	0.1604	0.0024	0.710
650	0.0329	0.1592	0.0280	0.734
660	0.0328	0.1581	0.1996	0.756
670	0.0327	0.1558	0.4890	0.777
680	0.0328	0.1555	0.6809	0.797
690	0.0328	0.1554	0.7875	0.816
700	0.0328	0.1553	0.8304	0.834
710	0.0328	0.1552	0.8451	0.851
720	0.0329	0.1551	0.8668	0.867
730	0.0329	0.1550	0.9016	0.882
740	0.0329	0.1552	0.9519	0.895
750	0.0330	0.1567	0.9921	0.908
760	0.0331	0.1567	1.0000	0.920
770	0.0331	0.1565	0.9711	0.931
780	0.0331	0.1561	0.9283	0.941
790	0.0331	0.1560	0.8966	0.950
800	0.0331	0.1557	0.8875	0.959
810	0.0332	0.1556	0.8975	0.966
820	0.0332	0.1556	0.9137	0.973
830	0.0333	0.1558	0.9226	0.979

840	0.0333	0.1558	0.9091	0.984
850	0.0333	0.1556	0.8702	0.988
860	0.0334	0.1554	0.7991	0.992
870	0.0333	0.1553	0.7311	0.995
880	0.0334	0.1556	0.6684	0.997
890	0.0334	0.1529	0.6076	0.999
900	0.0334	0.1529	0.5574	1.000
910	0.0334	0.1531	0.5036	1.000
920	0.0334	0.1529	0.4555	1.000
930	0.0334	0.1523	0.4123	0.999
940	0.0334	0.1524	0.3744	0.998
950	0.0332	0.1531	0.3401	0.996
960	0.0334	0.1537	0.3067	0.993
970	0.0336	0.1544	0.2776	0.991
980	0.0337	0.1551	0.2479	0.987
990	0.0338	0.1555	0.2166	0.984
1000	0.0338	0.1557	0.1850	0.979
1010	0.0339	0.1561	0.1528	0.975
1020	0.0340	0.1562	0.1220	0.970
1030	0.0340	0.1562	0.0940	0.965
1040	0.0341	0.1564	0.0716	0.959
1050	0.0341	0.1563	0.0519	0.953
1060	0.0341	0.1563	0.0378	0.947
1070	0.0342	0.1567	0.0281	0.941
1080	0.0345	0.1561	0.0224	0.934
1090	0.0345	0.1558	0.0177	0.927
1100	0.0345	0.1562	0.0138	0.920

When these values are used, the ratio of the spatial function in equation (11) for the anodized aluminum and Krylon painted parts of the target are 4.68. Thus, any part of the target painted with Krylon needs to be boosted by this factor to put the spatial function for the lamp to the same scale as that derived from the anodized part of the target.

Once the spatial distribution function for the pattern of light from the SSL has been found, the spectrum of the target observed by the DLIS can be used to find the absolute spectral flux at the brightest part of the lamp pattern. The net count rate from the DLIS spectrum is related to the lamp brightness by

$$DN/\sec = Resp_{peak}(\lambda)\frac{\mathbf{F}_P(\lambda)}{\pi} \Big/ \left[R_1(\lambda)\int Rel(\vartheta,\varphi)F'(\vartheta,\varphi)R_1'(\vartheta,\varphi)d\Omega + R_2(\lambda)\int Rel(\vartheta,\varphi)F'(\vartheta,\varphi)R_2'(\vartheta,\varphi)d\Omega\right] \quad (12.)$$

where $R_1(\lambda)$ and $R_2(\lambda)$ are the spectral reflectivities of Krylon and anodized aluminum, respectively, and R_1' is an array that is unity in the Krylon part of the target and zero elsewhere while R_2'is unity in the anodized part of the target and zero elsewhere.

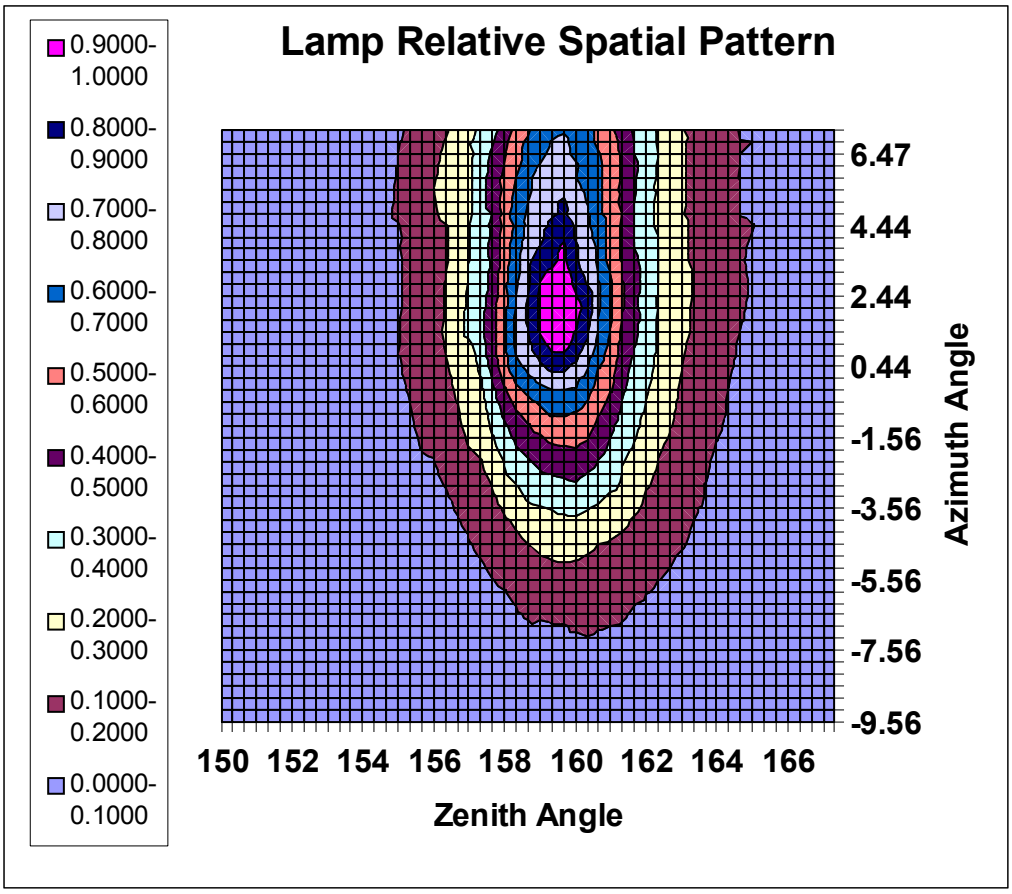

Fig. 9 The relative spatial output of the Surface Science Lamp determined from a combination of the Medium Resolution Imager (MRI) and the High Resolution Imager (HRI). The zenith and azimuth angle scales are for the MRI imager. Note that an azimuth of –2.56 degrees corresponds to an azimuth of 0 degrees in the DLIS FOV for observations at 4.68 m distance. At Titan, an azimuth of –1.5 degree in this plot corresponds to an azimuth of 0 degrees for the DLIS FOV.

Recall that during the absolute calibration measurement in the integrating sphere, the operating equation for the DLIS was given by

$$DN/\sec = Resp_{peak}(\lambda) I(\lambda) \int Rel(\vartheta,\varphi) d\Omega \,. \qquad (13.)$$

In the integrating sphere, the proportionality factor between the intensity I(λ) and the net count rate was taken as the measured responsivity. Thus the measured responsivity, $Resp_m(\lambda)$ is

$$Resp_m(\lambda) = Resp_{peak}(\lambda) \int Rel(\vartheta,\varphi) d\Omega \,. \qquad (14.)$$

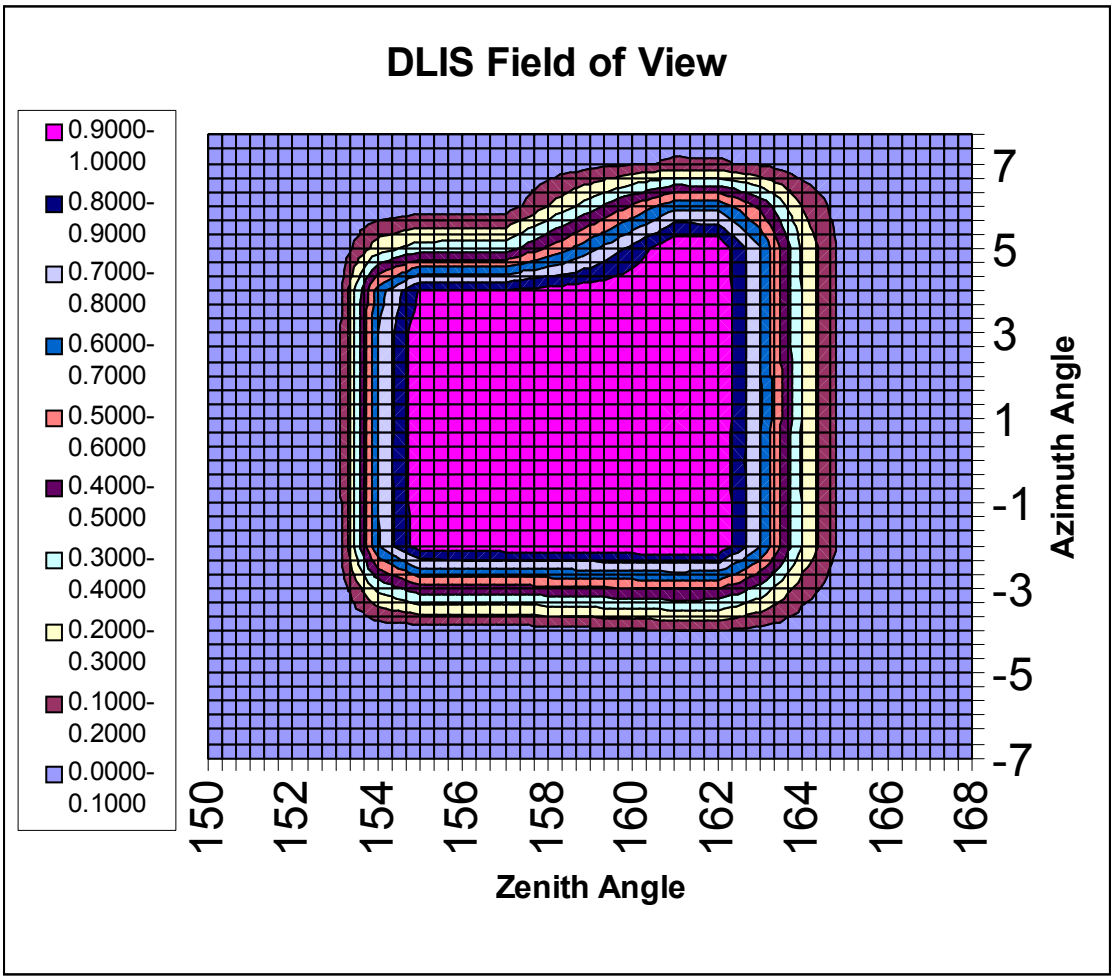

Fig. 10 The field of view (FOV) of the DLIS slit on DISR03 as formed by extrapolation of the three cuts across the FOV measured using the collimator. The three cuts are made in azimuth at zenith angles of 157 and 161 degrees, and in zenith at an azimuth angle of 0 degrees.

From the measurements over the field of view of the DLIS, the integral over the slit is 9.116×10^{-3} ster. Thus, the peak response over the slit is the measured response divided by this value.

The integrals of the relative response times the spatial distribution of the lamp pattern times the fraction of the area covered by Krylon paint in equation (7) is 8.11×10^{-6} ster, and the integral over the anodized portion of the target is 2.445×10^{-3} ster. Thus the spectral flux from the lamp at the brightest part of the pattern is given by

$$\mathbf{F}_P(\lambda) = \pi \frac{DN/\sec(\lambda)}{Resp_{peak}(\lambda)\left[R_{Krylon}(\lambda)8.11x10^{-6} + R_{anodized}(\lambda)2.445x10^{-3}\right]}. \qquad (15.)$$

Alternatively, the net count rate can be converted to an intensity, or

$$I(\lambda) = \frac{DN/\sec(\lambda)}{Resp_m(\lambda)}. \qquad (16.)$$

With this expression and the relation between the peak and measured response, equation (15) becomes

$$\mathbf{F}_P(\lambda) = \pi \frac{I(\lambda)\int Rel(\vartheta,\varphi)d\Omega}{\left[R_{Krylon}(\lambda)8.896x10^{-4} + R_{anodized}(\lambda)2.682x10^{-1}\right]}. \qquad (17.)$$

Using the value of $9.116x10^{-3}$ ster for the integral of the relative spatial response of the DLIS over its slit gives the spectral flux from the SSL at the peak of its spatial pattern from the spectral reflectivities of the Krylon and anodized aluminum times the reflectivity of the spectraflect reflectance standard. The results are shown in Table 4 below and Fig.11 below.

Table 4
Spectral Flux from SSL at Peak of Pattern

Pixel	Wavelength (nm)	R(λ) Krylon	R(λ) Anodized	I(λ)	I(λ)	Flux(λ)	Flux(λ)
9	850.0	0.0316	0.1513	0.2671	0.2553	19.76	20.67
10	857.1	0.0317	0.1519	0.2676	0.2450	18.88	20.62
11	864.2	0.0317	0.1526	0.2681			20.57
12	871.3	0.0318	0.1532	0.2687	0.2662	20.34	20.53
13	878.4	0.0318	0.1535	0.2693	0.2080	15.87	20.54
14	885.5	0.0319	0.1531	0.2700	0.2669	20.41	20.64
15	892.6	0.0319	0.1528	0.2706	0.2708	20.75	20.74
16	899.6	0.0320	0.1526	0.2713	0.2740	21.01	20.81
17	906.7	0.0320	0.1530	0.2720	0.2743	21.00	20.82
18	913.8	0.0321	0.1530	0.2727	0.2776	21.24	20.86
19	920.8	0.0321	0.1527	0.2733	0.2707	20.75	20.96
20	927.8	0.0320	0.1519	0.2740			21.11
21	934.9	0.0319	0.1517	0.2746	0.2626	20.26	21.18
22	941.9	0.0320	0.1521	0.2752	0.2738	21.08	21.18
23	948.9	0.0322	0.1527	0.2757	0.2729	20.93	21.14
24	955.9	0.0322	0.1532	0.2762	0.2782	21.26	21.10
25	962.9	0.0323	0.1537	0.2766	0.2230	16.98	21.07
26	969.9	0.0325	0.1542	0.2770			21.03
27	976.9	0.0326	0.1546	0.2773	0.2404	18.20	20.99
28	983.9	0.0326	0.1550	0.2775	0.2299	17.36	20.96
29	990.8	0.0326	0.1552	0.2777			20.95
30	997.8	0.0327	0.1553	0.2778	0.2635	19.86	20.94
31	1004.8	0.0328	0.1556	0.2778	0.2625	19.75	20.91
32	1011.7	0.0328	0.1559	0.2778	0.2495	18.74	20.86
33	1018.6	0.0328	0.1560	0.2776	0.2440	18.31	20.83
34	1025.6	0.0328	0.1559	0.2774	0.2736	20.55	20.83
35	1032.5	0.0328	0.1558	0.2771	0.2749	20.65	20.82
36	1039.4	0.0328	0.1559	0.2768	0.2749	20.64	20.78
37	1046.3	0.0329	0.1561	0.2763	0.2697	20.23	20.73

38	1053.2	0.0329	0.1561	0.2758	0.2749	20.62	20.69
39	1060.1	0.0329	0.1559	0.2752	0.2752	20.67	20.67
40	1067.0	0.0328	0.1558	0.2744	0.2776	20.86	20.62
41	1073.8	0.0328	0.1557	0.2737	0.2311	17.37	20.58
42	1080.7	0.0328	0.1556	0.2728	0.2573	19.36	20.53
43	1087.6	0.0328	0.1556	0.2718	0.2732	20.55	20.45
44	1094.4	0.0327	0.1555	0.2708	0.2761	20.78	20.38
45	1101.2	0.0327	0.1554	0.2697	0.2709	20.41	20.32
46	1108.1	0.0327	0.1554	0.2685	0.2688	20.25	20.23
47	1114.9	0.0327	0.1554	0.2673	0.2542	19.15	20.14
48	1121.7	0.0326	0.1553	0.2659	0.2530	19.07	20.04
49	1128.5	0.0326	0.1552	0.2645			19.95
50	1135.3	0.0326	0.1551	0.2630			19.85
51	1142.1	0.0326	0.1550	0.2615	0.2494	18.84	19.75
52	1148.9	0.0326	0.1547	0.2599	0.2514	19.02	19.66
53	1155.7	0.0326	0.1544	0.2582	0.2506	19.00	19.57
54	1162.4	0.0325	0.1541	0.2565	0.2537	19.27	19.48
55	1169.2	0.0324	0.1536	0.2547	0.2502	19.06	19.40
56	1175.9	0.0323	0.1533	0.2528	0.2526	19.29	19.30
57	1182.7	0.0322	0.1530	0.2509	0.2486	19.02	19.20
58	1189.4	0.0322	0.1527	0.2490	0.2198	16.85	19.09
59	1196.1	0.0322	0.1526	0.2470			18.95
60	1202.8	0.0322	0.1525	0.2449			18.80
61	1209.6	0.0321	0.1523	0.2428	0.2385	18.34	18.67
62	1216.3	0.0321	0.1522	0.2407	0.2390	18.38	18.51
63	1223.0	0.0320	0.1522	0.2386			18.35
64	1229.6	0.0321	0.1521	0.2364	0.2354	18.11	18.19
65	1236.3	0.0321	0.1522	0.2342	0.2320	17.84	18.02
66	1243.0	0.0320	0.1523	0.2320	0.2344	18.03	17.84
67	1249.7	0.0321	0.1524	0.2297	0.2284	17.55	17.65
68	1256.3	0.0321	0.1525	0.2275	0.2292	17.59	17.46
69	1262.9	0.0323	0.1532	0.2252			17.21
70	1269.6	0.0326	0.1547	0.2229	0.2270	17.18	16.87
71	1276.2	0.0329	0.1562	0.2206	0.2236	16.76	16.54
72	1282.8	0.0330	0.1569	0.2184			16.29
73	1289.4	0.0327	0.1558	0.2161	0.2179	16.38	16.24
74	1296.1	0.0323	0.1539	0.2137	0.2176	16.55	16.26
75	1302.7	0.0319	0.1519	0.2115	0.2121	16.34	16.29
76	1309.2	0.0316	0.1501	0.2092	0.2118	16.51	16.31
77	1315.8	0.0313	0.1486	0.2069	0.2066	16.27	16.30
78	1322.4	0.0310	0.1474	0.2047	0.2053	16.30	16.25
79	1329.0	0.0308	0.1464	0.2024	0.2006	16.04	16.18
80	1335.5	0.0306	0.1457	0.2002	0.1982	15.93	16.09
81	1342.1	0.0305	0.1451	0.1980	0.1872	15.10	15.98
82	1348.6	0.0304	0.1447	0.1959	0.1701	13.76	15.85
83	1355.1	0.0303	0.1445	0.1937	0.1465	11.87	15.70
84	1361.7	0.0302	0.1442	0.1916	0.1375	11.16	15.55
85	1368.2	0.0302	0.1439	0.1895	0.1424	11.59	15.42
86	1374.7	0.0302	0.1438	0.1875	0.1454	11.83	15.26
87	1381.2	0.0302	0.1438	0.1855	0.1442	11.74	15.10
88	1387.7	0.0301	0.1435	0.1835	0.1504	12.26	14.97
89	1394.2	0.0300	0.1436	0.1816	0.1466	11.95	14.81
90	1400.7	0.0300	0.1437	0.1797	0.1384	11.28	14.64

91	1407.1	0.0301	0.1435	0.1779	0.1491	12.16	14.51
92	1413.6	0.0300	0.1434	0.1761	0.1555	12.70	14.37
93	1420.0	0.0300	0.1433	0.1743	0.1569	12.81	14.24
94	1426.5	0.0299	0.1430	0.1726	0.1599	13.08	14.13
95	1432.9	0.0298	0.1426	0.1709	0.1581	12.98	14.03
96	1439.3	0.0297	0.1421	0.1693	0.1596	13.15	13.95
97	1445.8	0.0296	0.1419	0.1677	0.1573	12.98	13.84
98	1452.2	0.0296	0.1419	0.1662	0.1609	13.27	13.71
99	1458.6	0.0296	0.1419	0.1647	0.1592	13.13	13.59
100	1465.0	0.0295	0.1417	0.1633	0.1589	13.12	13.49
101	1471.3	0.0295	0.1417	0.1619			13.38
102	1477.7	0.0296	0.1421	0.1606	0.1569	12.93	13.23
103	1484.1	0.0296	0.1422	0.1593			13.12
104	1490.5	0.0297	0.1422	0.1581			13.01
105	1496.8	0.0297	0.1426	0.1569	0.1567	12.87	12.88
106	1503.2	0.0297	0.1429	0.1557	0.1572	12.88	12.76
107	1509.5	0.0297	0.1431	0.1546	0.1554	12.72	12.65
108	1515.8	0.0297	0.1430	0.1535			12.57
109	1522.2	0.0297	0.1431	0.1525	0.1253	10.25	12.48
110	1528.5	0.0298	0.1436	0.1515	0.1541	12.56	12.35
111	1534.8	0.0298	0.1437	0.1506	0.1517	12.36	12.27
112	1541.1	0.0297	0.1436	0.1496	0.1516	12.36	12.19
113	1547.4	0.0298	0.1436	0.1487	0.1492	12.16	12.12
114	1553.7	0.0297	0.1436	0.1478	0.1488	12.13	12.05
115	1559.9	0.0297	0.1436	0.1470	0.1474	12.01	11.98
116	1566.2	0.0297	0.1438	0.1462	0.1471	11.97	11.90
117	1572.5	0.0297	0.1439	0.1453	0.1445	11.76	11.82
118	1578.7	0.0297	0.1438	0.1445	0.1459	11.88	11.77
119	1584.9	0.0296	0.1439	0.1437	0.1196	9.74	11.70
120	1591.2	0.0296	0.1439	0.1429	0.1420	11.55	11.63
121	1597.4	0.0296	0.1439	0.1422	0.1394	11.34	11.56
122	1603.6	0.0296	0.1440	0.1414	0.1412	11.48	11.49
123	1609.8	0.0296	0.1441	0.1405	0.1337	10.86	11.42
124	1616.1	0.0296	0.1441	0.1397	0.1380	11.21	11.35
125	1622.2	0.0296	0.1442	0.1389	0.1372	11.14	11.27
126	1628.4	0.0296	0.1444	0.1380	0.1360	11.03	11.19
127	1634.6	0.0296	0.1446	0.1371	0.1342	10.87	11.10
128	1640.8	0.0296	0.1448	0.1361	0.1369	11.07	11.00
129	1646.9	0.0297	0.1446	0.1351			10.94
130	1653.1	0.0297	0.1446	0.1341	0.1345	10.89	10.86
131	1659.2	0.0297	0.1448	0.1330	0.1316	10.64	10.75
132	1665.4	0.0297	0.1444	0.1318	0.1388	11.25	10.68
133	1671.5	0.0296	0.1441	0.1305			10.60
134	1677.6	0.0296	0.1444	0.1292	0.1399	11.34	10.48
135	1683.7	0.0296	0.1446	0.1278	0.1443	11.69	10.35
136	1689.8	0.0296	0.1448	0.1262	0.1508	12.20	10.21
137	1695.9	0.0297	0.1453	0.1246	0.1540	12.41	10.04
138	1702.0	0.0298	0.1459	0.1229	0.1786	14.33	9.86
139	1708.1	0.0298	0.1466	0.1210			9.66
140	1714.2	0.0297	0.1467	0.1189	0.2189	17.47	9.49

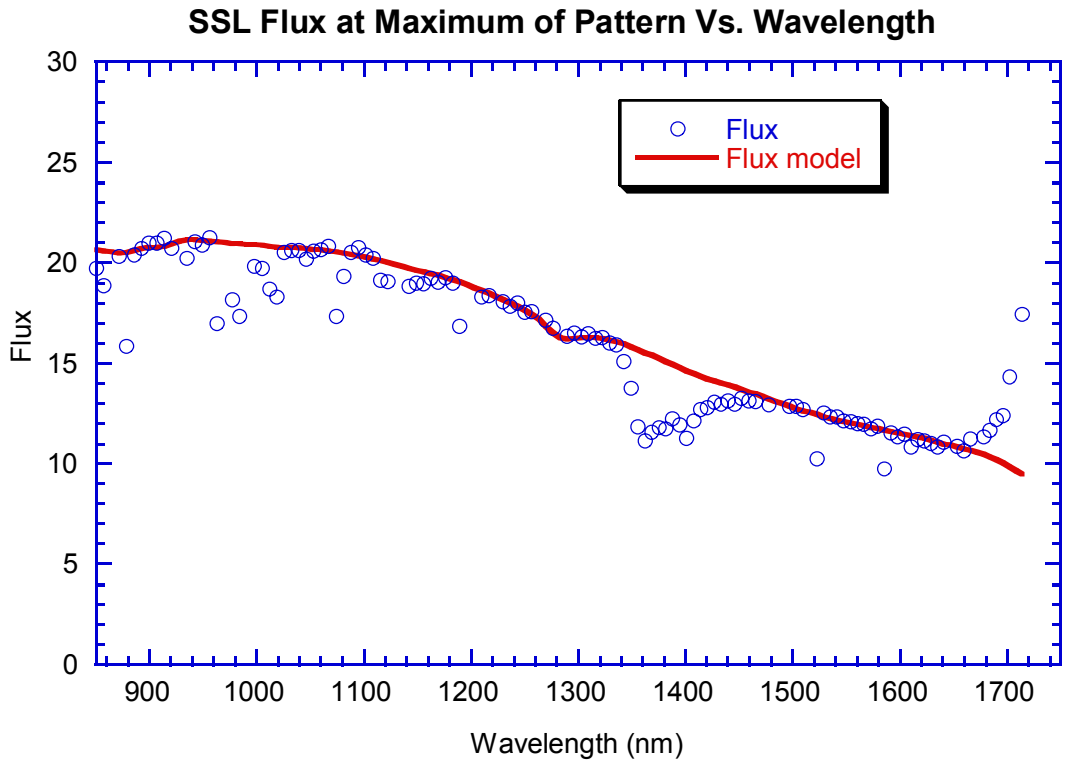

Fig. 11 Spectral flux output of the lamp is shown at the maximum of the lamp pattern. The circles are from the direct measurements of intensity, and show features due to water absorption in the laboratory at 1400 nm, 1120 nm, and near 950 nm. Several points are also below the general level of the curve due to the long integration time used at a warm temperature that resulted in several of the pixels in the spectrum being saturated. The upper smooth curve is an estimate of the lamp spectrum without saturation and absorption by water vapor in the 4.68 m path between the lamp and the target.

As noted in Fig.11, several of the points in the DLIS spectrum of the lamp are below the general level of the other points. This is due to the long integration time between readouts used for these measurements at the relatively warm temperature of the laboratory which caused saturation of some pixels. Also seen are absorption features near 1400 nm, 1120 nm and 950 nm by water vapor in the laboratory. The upper smooth curve estimates the spectral output of the lamp after these effects have been removed.

Once the absolute flux from the lamp at a standard distance is known along with the relative spatial lamp pattern and its integral over the DLIS slit, the count rate at any altitude for a surface with any spectral reflectivity can be computed. The count rate is given by

$$DN/\sec(\lambda) = Resp_{peak}(\lambda)\frac{\mathbf{F}_P(\lambda,)\cos(20)}{\pi}\left(\frac{4.68m}{z/\cos(20)}\right)^2 R(\lambda)\int F'(\vartheta,\varphi)Rel(\vartheta,\varphi)d\Omega\,. \quad (18.)$$

The integral of the spatial function with the relative spatial response is 2.98×10^{-3} ster when the parallax in the lamp at close range is corrected to the situation for targets in the far field at Titan

Finally, we must include the contribution from light from the SSL scattered within the instrument. At the measured distance of 4.68 m, the contribution of scattered light was measured by covering the entrance window of the DLIS. The result showed that the signal had a distribution with wavelength like that from the lamp, and was 0.0055 times the signal from the target at a range of 4.68 m. This implies that this fixed signal will be equal to the signal reflected from the surface at an altitude of about 63 m. The total count rate including this contribution from scattered light is shown in Fig. 2. for a ground with a flat reflectivity of 10%. Note that the lamp is turned on at 700 m altitude, and that the scattered light signal will be well determined between 700 m and some 200 m. At an altitude of 120 m, the total signal will be some 25% greater than that from scattered light alone (for R=0.1). At 60 m altitude, the total signal will be about twice that from scattered light, and at lower altitudes the signal from the surface will dominate the scattered light be ever larger factors. Figure 6 shows that reasonably good reflectance measurements are possible below about 100 m if the surface reflectivity is of the order of 10% or greater.

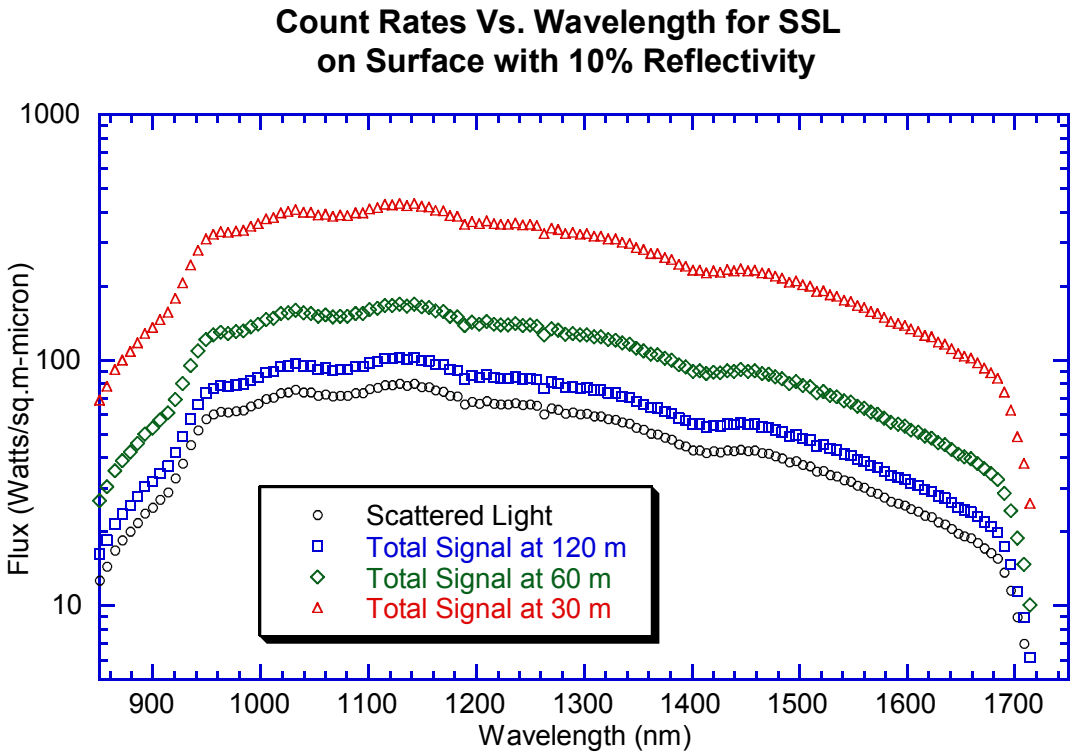

Fig. 12 Total count rate from light scattered within the instrument from the SSL and from the surface is shown as a function of wavelength at three altitudes of 120 m, 60 m, and 30 m. The curve for scattered light is also shown. Measurements of surface reflectivity good to some 4% of the surface reflectivity (0.004 for surface reflectivity of 0.10) are possible from altitudes of 120 m or less using the SSL at the peak of the response curve.